

Small Disks and Semiclassical Resonances

P. Rosenqvist and N. D. Whelan*

*Centre for Chaos and Turbulence Studies, Niels Bohr Institute, Blegdamsvej 17, DK-2100,
Copenhagen Ø, Denmark*

A. Wirzba

*Institut für Kernphysik, Technische Hochschule Darmstadt, Schloßgartenstr.9, 64289 Darmstadt,
Germany*

(November 15, 2018)

Abstract

We study the effect on quantum spectra of the existence of small circular disks in a billiard system. In the limit where the disk radii vanish there is no effect, however this limit is approached very slowly so that even very small radii have comparatively large effects. We include diffractive orbits which scatter off the small disks in the periodic orbit expansion. This situation is formally similar to edge diffraction except that the disk radii introduce a length scale in the problem such that for wave lengths smaller than the order of the disk radius we recover the usual semi-classical approximation; however, for wave lengths larger than the order of the disk radius there is a qualitatively different behaviour. We test the theory by successfully estimating the positions of scattering resonances in geometries consisting of three and four small disks.

PACS numbers: 0.320.+i, 03.65.Sq

Typeset using REVTeX

The presence of discontinuities in classical Hamiltonian systems implies the necessity of a closer study of the quantum mechanics when doing semiclassical periodic orbit theory [1] and has been the theme of numerous recent papers [2–9]. The approach is to study the quantum scattering problem near the discontinuity, combine this with classical information about classical trajectories away from the discontinuity to find global quantities such as the trace of the quantum Green function. In doing so, we maintain the local-global duality inherent in periodic orbit theory. In this paper we discuss one class of discontinuity, that of small circular scatterers. In the context of the Sinai billiard, the perturbative effect of a small disk in the quantum [10] and classical problems [11,12] was studied, but not with a scattering interpretation. By small, we mean smaller than the typical wavelength in the problem. The opposite limit, of scatterers much larger than a typical wavelength, can be evaluated using classical periodic orbits reflecting off the disk plus creeping diffraction to account for the discontinuity associated with glancing orbits [2–4,7].

We will analyse billiard systems in two dimensions and therefore seek the Green function of the Helmholtz equation

$$(\nabla^2 + k^2) \psi = 0 \quad (1)$$

with some specified boundary conditions. In the absence of any boundaries, the Green function between a source at x' and a receiver at x is

$$\begin{aligned} G_f(x, x', k) &= -\frac{i}{4} H_0^{(+)}(k|x - x'|) \\ &\approx \frac{1}{\sqrt{8\pi k|x - x'|}} e^{i(k|x - x'| - 3\pi/4)}. \end{aligned} \quad (2)$$

The second line, which is asymptotic in $k|x - x'|$, will be useful later in the discussion. In the exterior of a disk of radius a with Dirichlet boundary conditions, the first line of (2) is modified to

$$\begin{aligned} G(x, x', k) &= -\frac{i}{8} \sum_{m=-\infty}^{\infty} e^{im(\theta - \theta')} H_m^{(+)}(kx') \left(H_m^{(-)}(kx) - \frac{H_m^{(-)}(ka)}{H_m^{(+)}(ka)} H_m^{(+)}(kx) \right) \quad x' \geq x \\ &= G_f(x, x', k) + \frac{i}{4} \sum_{m=-\infty}^{\infty} e^{im(\theta - \theta')} \frac{J_m(ka)}{H_m^{(+)}(ka)} H_m^{(+)}(kx') H_m^{(+)}(kx), \end{aligned} \quad (3)$$

where θ and θ' are the polar angles of points x and x' as measured from the disk centre. The first line follows from using Graf's addition formula for $H_0^{(+)}(z)$ [13] together with the S-matrix of the disk scattering problem. The second line can be seen to equal the first by another application of Graf's addition formula and the expansion of $J_m(z)$ in terms of $H_m^{(\pm)}(z)$. If $x > x'$, one must interchange x with x' and θ with θ' in the first line of Eq. (3) but the second line rests unchanged. This has the appealing structure of being the free space Green function plus a correction. Whether the correction is small or large depends on the geometry of the problem and on the wave number k .

We now make the assumption that the disk radius a is much smaller than the typical distance to points x and x' from the disk. We further assume the semiclassical condition $kx, kx' \gg 1$. Recalling the asymptotic relation $H_m^{(+)}(z) \approx \exp(-im\pi/2)H_0^{(+)}(z)$ (assuming $|z| \gg 1$ and $|z| > m$), we obtain

$$\sum_{m=-\infty}^{\infty} e^{im(\theta-\theta')} \frac{J_m(ka)}{H_m^{(+)}(ka)} H_m^{(+)}(kx') H_m^{(+)}(kx) \approx H_0^{(+)}(kx') H_0^{(+)}(kx) \sum_{m=-\infty}^{\infty} e^{im(\theta-\theta'-\pi)} \frac{J_m(ka)}{H_m^{(+)}(ka)}. \quad (4)$$

Although the asymptotic forms used for $H_m^{(+)}(z)$ breaks down for $m > |z|$, this is not important in Eq. (4) since the condition $x, x' \gg a$ implies that the breakdown begins for values of m such that the factor $J_m(ka)/H_m^{(+)}(ka)$ is already very small. We then conclude that in the presence of a small disk centred at position ξ , the Green function between two points separated by an angle ϕ as measured from ξ is approximately

$$G(x, x', k) \approx G_f(x, x', k) + d(\phi) G_f(x, \xi, k) G_f(\xi, x', k) \quad (5)$$

where we have defined a diffraction constant

$$d(\phi) = -4i \sum_{m=-\infty}^{\infty} e^{im(\phi-\pi)} \frac{J_m(ka)}{H_m^{(+)}(ka)}. \quad (6)$$

Using the relations $J_{-m}(z) = (-1)^m J_m(z)$ and $H_{-m}^{(+)}(z) = (-1)^m H_m^{(+)}(z)$, we can replace the exponentials in this expression by cosines thereby displaying the time-reversal property $d(\phi) = d(-\phi)$. Furthermore, this sum converges since the ratio $J_m(ka)/H_m^{(+)}(ka)$ decreases

factorially with m for $m > |ka|$. In the more general case of a non-circular but small scatterer, we must insert the full S matrix into Eq. (3). The analysis remains largely unchanged; in particular Eq. (5) still applies however the diffraction constant is then a function of both angles and not just their difference. We then obtain

$$d(\theta, \theta') = 2 \sum_{m, m'=-\infty}^{\infty} e^{i(m'\theta - m\theta' - (m+m')\pi/2)} T_{mm'}, \quad (7)$$

where we have defined the S matrix through $S_{mm'} = \delta_{mm'} - iT_{mm'}$.

The Green function (5) has a direct contribution as if there were no disk plus a contribution in the form of a product of Green functions which arises from scattering off the disk. This is the same structure which exists in the presence of vertices [14] where we obtain the diffraction constant from the solution of the wedge scattering problem solved by Sommerfeld [15]. Despite the similar form, there are two aspects of the problems which are quite different. The small disk diffractor has no internal orientation but does have an internal length scale, a . In contrast, a wedge has an internal orientation, as given by the direction of its normal, but has no internal length scale. The existence of an orientation means that there are choices of incoming and outgoing angles for which the vertex diffraction constant diverges whereas this never happens for the disk. On the other hand, the lack of an internal length scale means that the vertex diffraction constant is independent of k whereas for the disk it is clearly k -dependent. The systems do share the property that we can trivially extend them to include problems with a potential $V(x)$ [9]. We assume that the potential does not change much in a wavelength and thereby compute the diffraction constant with $k = \sqrt{2m(E - V(\xi))/\hbar}$, the wave number at the disk. Eqs. (5) and (6) then apply where G_f is the Van-Vleck approximation to the Green function for that potential in the absence of a disk.

So far we have made no assumption on the value of ka . For $ka \gg 1$ we recover the expected geometrical structure, as we discuss below. There is qualitatively different behaviour for $ka \ll 1$ and a cross-over for $ka \sim 1$. In the limit $ka \rightarrow 0$ we note that $J_m(ka)/H_m^{(+)}(ka) \approx i\pi(ka/2)^{2m}/m!(m-1)!$ for $m \neq 0$ and only the $m = 0$ term contributes

significantly. We call this the s-wave limit. From the approximations

$$J_0(ka) \approx 1 \quad Y_0(ka) \approx \frac{2}{\pi} \left(\log \left(\frac{ka}{2} \right) + \gamma_e \right) \quad (8)$$

valid for small ka (where $\gamma_e = 0.577 \dots$ is Euler's constant), we derive the s-wave approximation

$$d \approx \frac{2\pi}{\log \left(\frac{2}{ka} \right) - \gamma_e + i\frac{\pi}{2}}, \quad (9)$$

which is independent of scattering angle ϕ . As $ka \rightarrow 0$, the denominator of Eq. (9) grows logarithmically so that the diffraction constant goes to zero and the disk has no effect, which is reasonable. However, this happens very slowly so that even for very small values of ka there is still an appreciable effect, as we will demonstrate.

It might seem surprising that the diffraction constant vanishes as $a \rightarrow 0$ since we are demanding that the wave function vanish at a point, and it might be thought that this should have some effect. That this is not so can be understood with the example of an annulus in which the central disk is very small. Although the eigenfunction does indeed vanish on the disk, it increases very rapidly so that within a small distance the eigenfunction is indistinguishable from one in which there were no central disk. In this sense, the wavefunctions (and eigenvalues) are virtually indistinguishable from those corresponding to the disk-free system. In Ref. [16], the author argues that disks of zero radius continue to have an effect, but the system he was considering was equivalent to an infinitely thin line charge in an electro-magnetic wave guide (see also Ref. [17] for the three dimensional generalisation.) In his language, our disk is uncharged and there is no contradiction between his conclusions and ours. The difference is in the order one takes the limits $a \rightarrow 0$ and $k \rightarrow \infty$. In Ref. [16], one starts with the first limit (while maintaining a finite interaction) whereas we consider the second limit while holding a small but fixed. As a result, the problems are quite distinct. For example, in the short wavelength limit the disks considered here will start having a large, classical effect (i.e. when ka is of order 1) whereas in the system mentioned above the effect of the scatterer vanishes for large k [18].

In a system composed of several scattering centres, the Green function between points labelled x' and x will receive contributions from paths which diffract several times. The contribution of one such path, labelled p , is a simple generalisation of the second term of (5) and equals

$$G_p(x, x', k) \approx G_f(x, \xi_n, k) d_n \left\{ \prod_{j=1}^{n-1} G_f(\xi_{j+1}, \xi_j, k) d_j \right\} G_f(\xi_1, x', k). \quad (10)$$

The quantities ξ_j indicate the scattering points - in this case the centres of the disks with the subscripts j indicating the order in which they are encountered for that path. The path is composed of n scatterers with a diffraction constant d_j associated with each one. The details of the trace integral are worked out in Refs. [3,6,9]; here we simply sketch the derivation. We stress that all of these calculations are to leading order in \hbar (or $1/k$ in this context.) The criterion of stationary phase selects periodic orbits which are everywhere classical except at the singularities where they diffract by an arbitrary angle. A periodic orbit is composed of n classical segments connected by n diffractions.

If we identify x with x' in (10) we see that it is a closed cycle of Green functions in which the segment between the scatterers ξ_n and ξ_1 is “cut” by the point x which lies between them. In general, the trace integral associated with a periodic orbit labelled γ will be evaluated by integrating over all choices of x . This means that we must allow x to cut open the cycle of Green’s functions between any two consecutive scatterers - each possibility physically corresponds to x lying between that pair of scatterers. For this purpose, we define a parallel coordinate z which runs along the periodic orbit from ξ_n to ξ_1 to ξ_2 etc. until it returns to ξ_n . When z is between ξ_i and ξ_{i+1} , the point x is between these two scatterers (where we identify $n + 1$ with 1.) At each point along the orbit, we define a transverse coordinate y so that x is parameterised by the pair (y, z) , as for geometric orbits [1]. The integrand of the trace integral is similar to (10) but where we cut the cycle of Green’s functions between ξ_i and ξ_{i+1} (as governed by z) rather than between ξ_n and ξ_1 so that the trace integral associated with γ is

$$\oint dz \int dy G_\gamma(x, x, k) = \sum_{i=1}^n \int_{\xi_i}^{\xi_{i+1}} dz \int_{-\infty}^{\infty} dy G_f(x, \xi_i, k) d_i \left\{ \prod_{j \neq i} G_f(\xi_{j+1}, \xi_j, k) d_j \right\} G_f(\xi_{i+1}, x, k). \quad (11)$$

Due to stationary phase, only those points close to the orbit contribute significantly so that to leading order, all the diffraction constants d_j are independent of x and can be considered invariant properties of the periodic orbit. Therefore, the only x dependence is in the two Green functions connecting x to the adjacent scatterers; all other factors in the integrand are constant. For each value of z , we evaluate the transverse integral $\int dy$ by stationary phase; this yields a factor which is independent of z and is proportional to the Green function between the two adjacent scatterers. Combining this with all the constant factors in the integrand gives the product of the closed cycle of Green functions and diffraction constants from one scatterer to the next, $\prod_{j=1}^n G_f(\xi_{j+1}, \xi_j, k) d_j$. We get this same invariant factor after doing the y integral at any point z along any segment of the periodic orbit so there is no explicit z dependence remaining. The integral parallel to the orbit $\oint dz = L_\gamma$ is then simply the length of the periodic orbit, as also happens for geometric orbits. The final result is

$$\begin{aligned} g_\gamma(k) &\approx -i \frac{L_\gamma}{2k} \left\{ \prod_{j=1}^{n_\gamma} G_f(\xi_{j+1}, \xi_j) d_j \right\} \\ &\approx -i \frac{L_\gamma}{2k} \left\{ \prod_{j=1}^{n_\gamma} \frac{d_j}{\sqrt{8\pi k L_j}} \right\}_\gamma \exp\{i(kL_\gamma - 3n_\gamma\pi/4)\}. \end{aligned} \quad (12)$$

We have made use of (2) where $L_j = |\xi_{j+1} - \xi_j|$. This expression involves one fewer Green function than (10). (The additional Green function contributes a constant proportional to $e^{-i3\pi/4}/\sqrt{k}$ which combines with a factor proportional to $e^{i\pi/4}/\sqrt{k}$ from the stationary phase integral to give the prefactor of $-i/2k$.) Eq. (12) is the contribution of a single diffractive periodic orbit, in general we must sum over all such orbits as well as over all purely geometric orbits to get the total trace. For this reason, we have introduced the subscript γ on the index n_γ in the above equation.

Following Refs. [3,4,8] we write down the semiclassical diffractive zeta function [19] whose zeros approximate the exact quantum resonances,

$$\zeta_{\text{diff}}^{-1} = \prod_{\gamma} (1 - t_{\gamma}) \quad (13)$$

where

$$t_{\gamma} = \left\{ \prod_{j=1}^n \frac{d_j}{\sqrt{8\pi k L_j}} \right\}_{\gamma} \exp\{i(kL_{\gamma} - 3n_{\gamma}\pi/4)\} \quad (14)$$

This results follows from the semiclassical approximation

$$\frac{dt_{\gamma}}{dk^2} \approx \frac{iL_{\gamma}}{2k} t_{\gamma} \quad (15)$$

so that the sum over all diffractive orbits in Eq. (12) is the logarithmic derivative of the zeta function (13). (We take the derivative with respect to k^2 since the trace of the Green function (12) is properly thought of as a function of k^2 and not of k .) The product is over just the primitive orbits; their repeats have already been summed. In a system with coexisting geometric and diffractive orbits, we need to multiply the corresponding zeta functions [3,4]. The result is a purely formal product which must be regulated differently for scattering [20–22] and bound [23] problems so that its zeros are the semiclassical eigenvalues of the full problem and not the zeros of the individual terms in the product. The diffractive zeta function (13) involves no additional product as happens for geometric orbits [24], resulting in there being only leading resonances in scattering calculations [5,8].

We now specialise the discussion to scattering geometries featuring three and four small disks arranged symmetrically in the plane [25–32]. We first discuss the three disk problem as shown in Fig. 1a (we exaggerate the size of the disks to make the discussion clearer.) Starting from one of the disks, there are two distinct processes. We can go to one of the other two disks and either scatter back to the original disk or scatter on to the third disk. We assign these two processes the symbols 0 and 1 respectively [29]. The weights are $t_0 = d(0)u$ and $t_1 = d(\pi/3)u$ where the factor

$$u = \frac{1}{\sqrt{8\pi k R}} \exp\{i(kR - 3\pi/4)\} \quad (16)$$

is common to both orbits and $R \gg a$ is the inter-disk spacing.

Notice that there is a C_{3v} symmetry to this problem [27–30] consisting of the identity, rotations by $\pm 2\pi/3$ and reflections through the three symmetry axes. This group has three irreducible representations which are called A_1 , A_2 and E . We can make use of this symmetry by considering dynamics in the fundamental domain [33], which in this case is a wedge consisting of one sixth of the plane as indicated in Fig. 1a. One does this by following a trajectory and using the symmetry operations to map the trajectory back into the fundamental domain whenever it crosses a boundary. In the fundamental domain of the three disk problem, there is only one half disk. A trajectory can leave this half disk in only one direction, which is labelled A. Upon encountering the border of the fundamental domain, a reflection operation is applied so that the trajectory returns to the disk, where it has two choices. It can either diffract back onto A or it can diffract into the direction A'. In the second case, we apply a reflection operator again to map this back onto A. These two possibilities are both diffractive periodic orbits of the fundamental domain and have the weights t_0 and t_1 discussed above. Each orbit has an additional group theoretic weight given by the characters (in the representation being considered) of the group operations needed to keep the orbit in the fundamental domain [30].

In general there are longer periodic orbits as labelled by whether they back scatter or forward scatter at each encounter with the disk. These can be then labelled by a binary sequence of 0's and 1's. However, there is a multiplicative property to the weights such that the weight of any long orbit is equal to the product of the weights of shorter cycles. For example $t_{001} = t_0^2 t_1$ since they both equal $d_0^2 d_1 u^3$. This property means that we can represent the zeta function as being the determinant of a Markov graph [34], which is drawn in Fig. 1b. The single node in the graph, A, is connected to itself by the processes 0 and 1 described above.

All the characters of the totally symmetric representation A_1 are unity, which simplifies its discussion. To find its zeta function, we simply read off from the Markov graph all nonintersecting closed loops. In this case there are only two and we get the simple result

$$\zeta_{A_1}^{-1} = 1 - t_0 - t_1. \quad (17)$$

This formula agrees with the result found in Refs. [29,30] for the special case where all the higher order “curvature corrections” [20–22] vanish identically. This vanishing is simply a result of the fact that we have a one node graph so we only need consider weights of topological length one. Armed with this rule, we can then read off from Refs. [29,30] the zeta functions of the other two representations. These are

$$\zeta_{A_2}^{-1} = 1 + t_0 - t_1 \quad \zeta_E^{-1} = 1 + t_1 + t_1^2 - t_0^2. \quad (18)$$

We could have ignored the symmetry decomposition and simply drawn the six node Markov graph of the full problem as shown in Fig. 2. The vastly increased number of closed loops in comparison to Fig. 1 underlines the advantage of using the symmetry reduction. The rule for finding the zeta function is to find all non-intersecting closed loops and products of non-intersecting closed loops. A product of n non-intersecting closed loops has a relative sign $(-1)^n$. Carefully enumerating all such loops of the full graph, we find its zeta function to be

$$\zeta^{-1} = 1 - 3t_0^2 - 2t_1^3 + 3t_0^4 - 3t_0^2t_1^2 - t_0^6 + t_1^6 - 3t_0^2t_1^4 + 3t_0^4t_1^2. \quad (19)$$

This equals the product $\zeta_{A_1}^{-1}\zeta_{A_2}^{-1}\zeta_E^{-2}$ of the symmetry decomposed zeta functions above. In addition to the additional complexity of its Markov graph and zeta function, the full zeta function has the further disadvantage that we do not know to which symmetry class one of its zeros belongs. However, this exercise is useful in verifying that our use of the results of Ref. [29,30] is well founded.

The exact resonances of this geometry can be found numerically by finding the zeros of the determinant of a matrix. This matrix is [28]

$$M_{nm} = \delta_{nm} + A_{nm} \quad (20)$$

where for the A_1 resonances

$$A_{nm} = \frac{J_n(ka)}{H_m^{(+)}(ka)} \left[\cos\left(\frac{\pi}{6}(5n-m)\right) H_{n-m}^{(+)}(kR) + (-)^m \cos\left(\frac{\pi}{6}(5n+m)\right) H_{n+m}^{(+)}(kR) \right]. \quad (21)$$

Expressing $\det M$ in a cumulant expansion [2,35], valid because A is trace-class [35], yields

$$\det M = 1 + \text{tr} A - \frac{1}{2} (\text{tr} A^2 - (\text{tr} A)^2) + \dots \quad (22)$$

where from Eq.(21) one obtains [2]

$$\text{tr} A = \sum_{m=-\infty}^{\infty} \frac{J_m(ka)}{H_m^{(+)}(ka)} \left(\cos\left(\frac{2\pi m}{3}\right) H_0^{(+)}(kR) + H_{2m}^{(+)}(kR) \right). \quad (23)$$

We now impose the same constraints as before, namely $kR \gg 1$ and $R \gg a$ so that we can replace $H_{2m}^{(+)}(kR)$ by $\cos(m\pi)H_0^{(+)}(kR)$ and

$$\text{tr} A \approx H_0^{(+)}(kR) \sum_{m=-\infty}^{\infty} \frac{J_m(ka)}{H_m^{(+)}(ka)} (\cos(2\pi m/3) + \cos(m\pi)). \quad (24)$$

Then using Eqs.(6) and (16) and the asymptotic form of $H_0^{(+)}(kR)$, we find

$$\text{tr} A \approx -u (d(0) + d(\pi/3)) = -(t_0 + t_1). \quad (25)$$

We see that truncating the cumulant expansion at the term linear in A and invoking the relevant approximations gives the same equation for $\det M = 0$ as we earlier derived for $\zeta^{-1} = 0$. This is reassuring since it means that we understand the error caused by replacing $H_m^{(+)}(z)$ by $\exp(-im\pi/2)H_0^{(+)}(z)$ in Eqs.(4) and (24); it is the same as neglecting higher order terms in the cumulant expansion. As shown in Refs. [2,35], this is equivalent to neglecting higher order curvature corrections in the cycle expansion. The fact that the semiclassical approximation can be made on the level of the traces of the scattering kernel $\text{tr} A^n$ (21) which result from the defining cumulant expansion (22) provides an alternate method to arrive directly at the zeta function ζ_{diff}^{-1} . This method does not require closed expressions for the trace of the Green function, does not invoke the semiclassical relation (15) and, most importantly, appears in a curvature-regulated form [2,35]. In particular, one can use this to read the weights t_γ (14) directly from the Green's function product $\prod_{j=1}^n G_f(\xi_{j+1}, \xi_j, k) d_j$, which is just the closed path equivalent of the open path Green's function (10).

The identification between the quantisation conditions $\zeta_{A_1}^{-1} = 0$ and $\det M = 0$ tells us something else. In Ref. [2] it is shown that one can extract the contribution of geometric orbits and diffractive creeping orbits from $\text{tr} A$ by invoking Watson contour integration to replace the sum of Eq.(23). This means that the diffraction constant contains information about periodic orbits and creeping. Therefore, even in the limit $ka \gg 1$, the formalism described here still applies, the price being the necessity to include many terms in calculating the diffraction constant (6). We therefore have a uniform picture. For large values of ka , one invokes geometric and creeping orbits but for intermediate and small values one invokes the small disk scattering theory elucidated here. These are guaranteed to match smoothly. Although this was shown explicitly only for two and three disk systems, the same will hold for any number of disks in any geometrical arrangement.

We show the exact and semiclassical results in Fig. 3 for the A_1 and E resonances together with the approximations using geometric orbits. The resonances are shown in the complex k plane and are measured in units of $1/R$. In Fig. 3a we show the results for the A_1 resonances for $R/a = 60$ so that the cross-over condition $\text{Real}\{ka\} = 1$ corresponds to $\text{Real}\{kR\} = 60$. The minimum, which is developing at the right of the figure, has a geometrical interpretation in terms of interference between the two shortest geometrical orbits in the fundamental domain, t_0 and t_1 [27,29]. As promised, the diffractive picture captures this behaviour. For the highest values of k , we used 70 partial waves in the calculation of the diffraction constant (6). If we held the number of partial waves fixed, the calculation would start to fail for larger values of $|kR|$. We also include the results from the theory of geometrical orbits [29] for comparison. The new régime is at the left of the figure where $\text{Real}\{ka\} \ll 1$. There it can be seen that the widths of the resonances increase logarithmically with kR , a result which we generically expect for diffraction [5,8]. In those references it is shown that the width of the first resonance scales as $\log(d)$ and since d scales logarithmically with a , we find that the width of the first resonance (when measured in units of $1/R$) scales as $\log(\log(R/a))$, as opposed to the $\log(R/a)$ behaviour predicted by geometric orbits [2]. This means that in

the diffractive case, the resonances are observable even for extremely large values of R/a .

In Fig. 3b we show the results for the A_1 and E resonances for $R/a = 600$. The agreement conforms to the discussion of the top panel, however the increased value of R/a means that none of the resonances shown are in the geometrical régime $\text{Real}\{ka\} > 1$ so there is no strong interference between the weights t_0 and t_1 . The A_1 resonances have smaller widths because, to linear order, their zeta function (17) involves two weights, which are in phase, while the zeta function for the E resonances (18) involves only one weight. A disadvantage of the three disk problem for this study is that in the diffractive régime $ka \ll 1$ the s-wave term dominates so that the two diffraction constants $d(0)$ and $d(\pi/3)$ are very nearly equal and so too are the weights t_0 and t_1 . The result on the spectrum is approximately the same as if there were just one weight, a situation which is known to lead to rather uninteresting spectra [2,5]. For this reason we were led to study the four disk problem which we discuss next.

The four disk problem shown in Fig. 4a has more structure than the three disk because there are two distinct lengths in the problem; in addition to the side length R , there is the diagonal length $\sqrt{2}R$. Accordingly, we define the factor

$$v = \frac{1}{\sqrt{8\sqrt{2}\pi kR}} \exp\{i(\sqrt{2}kR - 3\pi/4)\}, \quad (26)$$

in analogy to u . In addition, there are now six distinct processes. Starting at any disk we can go to one of the two near disks and either diffract back with $d_0 = d(0)$, diffract to the next disk with $d_1 = d(\pi/2)$ or diffract diagonally with $d_2 = d(\pi/4)$. Additionally we can head diagonally across and diffract back with $d_3 = d(0)$ or to either one of the other two disks, again with $d_4 = d(\pi/4)$. This problem has C_{4v} symmetry which has four one dimensional representations labelled A_1 , A_2 , B_1 and B_2 and one two dimensional representation labelled E [30]. This system has previously been studied semiclassically using periodic geometric orbits [32].

As before, we want to find the Markov graph of the problem for which we study the dynamics in the fundamental domain which is one eighth of the full plane and is shown in

Fig. 4a. Starting at the half disk, we can go in one of two directions, which we call A and B . We want to find all paths which start and end at either A or B . From A we first reflect off the diagonal wall and upon returning either diffract back which we call 0, diffract to A' and then reflect onto A which we call 1 or diffract to B which we call 2. From B we first travel to the centre and on returning either diffract back which we call 3, diffract to A which we call 4 or diffract to A' and reflect to A which we call $\bar{4}$. This is shown diagrammatically as a Markov graph in Fig. 4b. Note that process 3 is a boundary orbit which lies on a symmetry axis and can be shown to contribute only to the spectra of representations which are not odd with respect to reflections through that axis [36].

The weights corresponding to each process involve one geometric arc and one diffraction so we find

$$t_0 = d_0 u \quad t_1 = d_1 u \quad t_2 = d_2 u \quad t_3 = d_3 v \quad t_4 = t_{\bar{4}} = d_4 v. \quad (27)$$

In general each one of these also has a group theoretic factor depending on the group representation being considered. Again, we start with the symmetric A_1 representation for which all the characters equal one. Enumerating all closed loops and products of closed loops on the graph, we read off the zeta function [19] as

$$\zeta_{A_1}^{-1} = 1 - t_0 - t_1 - t_3 - (2t_2 t_4 - t_0 t_3 - t_1 t_3) \quad (28)$$

where we have used the equality between t_4 and $t_{\bar{4}}$. This result involves cycles of topological lengths one and two. We now have contributions of length two since the graph has two nodes, however cycles of length three and higher are absent in Eq.(28). We again note that this is the same expression as the cycle expansion of the 4-disk problem discussed in Ref. [30] where we use $t_{01} = t_0 t_1$ and additionally invoke the identification between $\{t_0, t_1, t_3, t_2 t_4, t_2 t_{\bar{4}}, t_1 t_2 t_4, t_0 t_2 t_4\}$ in our notation and $\{t_0, t_1, t_2, t_{02}, t_{12}, t_{112}, t_{002}\}$ in theirs. As before, we can use this fact to read off the zeta functions of the other representations from Ref. [30],

$$\zeta_{B_2}^{-1} = 1 + t_0 + t_1 - t_3 + (2t_2 t_4 - t_0 t_3 - t_1 t_3)$$

$$\begin{aligned}
\zeta_{A_2}^{-1} &= 1 + t_0 - t_1 & \zeta_{B_1}^{-1} &= 1 - t_0 + t_1 \\
\zeta_E^{-1} &= 1 + t_3 + (t_1^2 - t_0^2) + (2t_0t_2t_4 - t_0^2t_3 - 2t_1t_2t_4 + t_1^2t_3).
\end{aligned} \tag{29}$$

We are primarily interested in the region $ka < 1$ for which the diffraction constants are almost equal (ie the s-wave limit) and we see that the A_2 and B_1 representations have almost total cancellation and therefore their resonances are comparatively deep in the complex k plane. These are the representations which are odd with respect to reflections across the diagonals of the square so process 3 does not contribute. Instead we concentrate on the representations A_1 , B_2 and E . In Fig. 5 we plot the exact positions of these three representations found using the algorithms of Refs. [35,37] together with the semiclassical approximations from Eqs. (28) and (29) for $R/a = 600$. In all cases, the semiclassical predictions from the zeta functions work well although it is interesting to note that there is a noticeable deterioration of the quality for the resonances with large imaginary part. The irreducible representations A_1 and B_2 have richer spectra due to the interferences among the three basic weights. The E resonances are given by a zeta function which is dominated by the weight t_3 and thereby shows the characteristic logarithmic behaviour discussed above and observed in Fig. 3a. For larger values of k , the quadratic terms of Eq. (29) become important leading to more structure in the E spectrum. This structure will eventually develop into the rich spectrum of scattered resonances predicted by the geometrical orbits.

In this problem, we have altogether defined 5 weights - however since t_2 and t_4 always occur as a product in the zeta functions, it is more precise to say there are 4 independent quantities. On the other hand, it is known that the geometric orbits can be labelled with just three symbols [30]. (In contrast, for the three disk problem we had only two weights, in agreement with the two symbols needed to label geometric periodic orbits.) This is reminiscent of the approximations of the transfer operator based on so-called T matrices [38] which lead to transcendental quantisation equations like (29) but in terms of classical trajectories. Increasing the dimension of the T matrices induces more complicated equations in terms of which the quantisation is more exact. That approximation is based on assuming

certain matrix elements (weights in our language) are approximately multiplicatively related and so drop out of the equations - as happens exactly for diffraction. The structural similarity between these results is presumably based on the underlying structure of finite Markov graphs which are used by us and are implicit in the work of [38].

In conclusion, we have discussed a form of discontinuity which is amenable to discussion in terms of diffraction, that of small disks. Since the effect of a disk vanishes as the disk radius goes to zero, we must consider disks of some fixed size. Doing so introduces a length scale in the problem such that if $ka \gg 1$ one can use standard geometrical optics. However in the domain $ka \ll 1$ a qualitatively new physical picture is necessary. The formalism we discuss here incorporates both limits but at the price of having to include many partial waves when $ka \gg 1$. We have tested this theory in systems consisting of three and four disks arranged symmetrically on the plane. The formalism of Markov graphs and zeta functions applies equally well to any system in which there exist objects which can be approximated as point singularities, including point scatterers mentioned above [16] and Aharonov-Bohm flux lines [39]. These systems allow a finite approximation based on zeta functions to give their scattering resonances and as such are formally useful in testing the formalism. However, the arguments developed here apply equally well to bound systems. Putting a small disk or other singularity inside a billiard introduces diffractive paths which appear in the Fourier transform of the spectrum [40] in a characteristic way, just as with edge diffraction [6,9].

The authors would like to thank Stephen Creagh and Predrag Cvitanović for useful discussions. A.W. would like to thank Predrag Cvitanović and the Centre for Chaos and Turbulence Studies at the Niels Bohr Institute for hospitality and support during his visit in August 1995. N.D.W. was supported by the European Union Human Capital and Mobility Fund.

REFERENCES

- * Present address: Division de Physique Théorique, IPN, 91406 Orsay Cedex, France.
- [1] M. C. Gutzwiller, *Chaos in Classical and Quantum Mechanics* (Springer Verlag, New York, 1990).
 - [2] A. Wirzba, Nucl. Phys. **A560**, 136 (1993).
 - [3] G. Vattay, A. Wirzba and P. E. Rosenqvist in *Proceedings of the International Conference on Dynamical Systems and Chaos: vol. 2*, edited by Y.Aizawa, S.Saito and K.Shiraiwa, p. 463 (World Scientific, Singapore, 1995).
 - [4] G. Vattay, A. Wirzba and P. E. Rosenqvist, Phys. Rev. Lett. **73**, 2304 (1994); P. E. Rosenqvist, G. Vattay and A. Wirzba, J. Stat. Phys. **83**, 243 (1996).
 - [5] N. D. Whelan, Phys. Rev. E **51**, 3778 (1995).
 - [6] N. Pavloff and C. Schmit, Phys. Rev. Lett. **75**, 61 (1995).
 - [7] H. Primack, H. Schanz, U. Smilansky and I. Ussishkin, Phys. Rev. Lett. **76**, 1615 (1996).
 - [8] N. D. Whelan, Phys. Rev. Lett. **76**, 2605 (1996).
 - [9] H. Bruus and N. D. Whelan, Nonlinearity **9**, 1 (1996).
 - [10] M. V. Berry, Ann. Phys. **131**, 163 (1981).
 - [11] B. Friedman, Y. Oono, and I. Kubo, Phys. Rev. Lett. **52**, 709 (1984).
 - [12] P. Dahlqvist, “The Lyapunov exponent in the Sinai billiard in the small scatter limit”, chao-dyn/9601007, (1996).
 - [13] Edited by M. Abramowitz and I. Stegun, *Handbook of Mathematical Functions* (Dover Publications, New York 1965).
 - [14] J. B. Keller, J. Appl. Phys. **28**, 426 (1957).

- [15] A. Sommerfeld, Mathem. Ann. **47**, 317 (1896); *Optics* (Academic Press, New York 1954).
- [16] P. Seba, Phys. Rev. Lett. **64**, 1855 (1990).
- [17] W. John, B. Milek, H. Schanz and P. Seba, Phys. Rev. Lett. **67**, 1949 (1991).
- [18] T. Cheon and T. Shigehara, “Scale Anomaly and Quantum Chaos in the Billiards with Pointlike Scatterers”, preprint, hep-th/9512162, (1995).
- [19] D. Ruelle, *Statistical Mechanics, Thermodynamic Formalism* (Addison-Wesley, Reading MA, 1978).
- [20] P. Cvitanović, Phys. Rev. Lett. **61**, 2729 (1988);
- [21] R. Artuso, E. Aurell and P. Cvitanović, Nonlinearity **3**, 325 (1990).
- [22] R. Artuso, E. Aurell and P. Cvitanović, Nonlinearity **3**, 361 (1990).
- [23] M. V. Berry and J. P. Keating, J. Phys. **A23**, 4389 (1990).
- [24] A. Voros, J. Phys. A **21**, 685 (1988).
- [25] B. Eckhardt, J. Phys. **A: Math Gen.** **20**, 5971 (1987).
- [26] P. Gaspard and S. Rice, J. Chem. Phys **90**, 2255 (1989).
- [27] P. Gaspard and S. Rice, J. Chem. Phys **90**, 2242 (1989).
- [28] P. Gaspard and S. Rice, J. Chem. Phys **90**, 2255 (1989).
- [29] P. Cvitanović and B. Eckhardt, Phys. Rev. Lett. **63**, 823 (1989).
- [30] P. Cvitanović and B. Eckhardt, Nonlinearity **6**, 277 (1993).
- [31] B. Eckhardt et. al., *Pinball Scattering*, in QUANTUM CHAOS BETWEEN ORDER AND DISORDER., eds. G. Casati and B. Chirikov, Cambridge University Press (1995).
- [32] P. Gaspard et. al., Phys. Rev. E **50**, 2591 (1994).

- [33] J. Robbins, Phys. Rev. A **40**, 2128 (1989).
- [34] see for example, P. Grassberger, Z. Naturforsch. **43a**, 671 (1988).
- [35] M. Henseler and A. Wirzba,
http://crunch.ikp.physik.th-darmstadt.de/~wirzba/#non_papers.
- [36] B. Lauritzen, Phys. Rev. A **43**, 603 (1991).
- [37] M. Henseler, diploma thesis: “Quantisierung eines chaotischen Systems: Die Streuung an N Kugeln und an N Kreisscheiben”, Institut für Kernphysik, TH Darmstadt, December (1995).
- [38] E. Bogomolny, Nonlinearity **5**, 805 (1992).
- [39] Y. Aharonov and D. Bohm, Phys. Rev. **115**, 485 (1959).
- [40] S. Reimann et. al., Phys. Rev. A **53**, 39 (1996).

FIGURES

FIG. 1. Left: The configuration space of the three disk problem with the fundamental domain indicated at the top right. The arrow A indicates the unique direction in which a trajectory can leave the disk and ultimately return and the arrow A' is its mirror image. Right: The corresponding Markov graph with a single node A and the two processes which connect it to itself.

FIG. 2. The same as Fig. 1 but without using the symmetry decomposition. There are now six possible directions and consequently a six node graph. The six short lines correspond to weights t_0 and the six long lines correspond to weights t_1 .

FIG. 3. Top: The A_1 three disk resonances for $R/a = 60$ plotted in the complex k plane. The exact resonances are represented as open circles, the semiclassical diffractive predictions as vertical crosses and the semiclassical geometric predictions as diagonal crosses. Bottom: The upper set of points are the A_1 resonances for $R/a = 600$ while the lower set are the E resonances. Same symbol convention but we do not include the geometrical orbit predictions. In both cases the wave numbers are measured in units of $1/R$.

FIG. 4. Left: The configuration space of the four disk problem with the fundamental domain indicated. The two available directions are A and B and A' is the mirror image of A . Right: The corresponding Markov graph with two nodes A and B and all the interconnecting processes.

FIG. 5. Top: The A_1 resonances of the four disk problem for $R/a = 600$. Middle: The B_2 resonances. Bottom: The E resonances. (Same symbol and unit convention as in Fig. 3.)

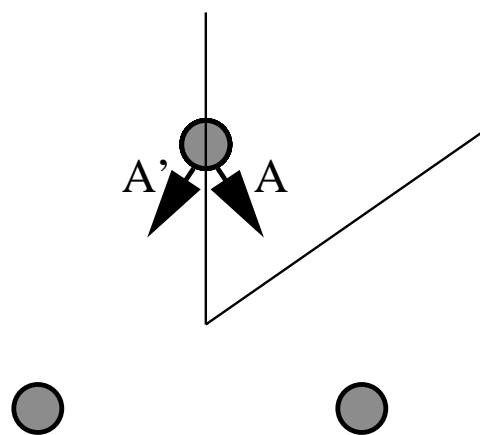


Fig. 1a

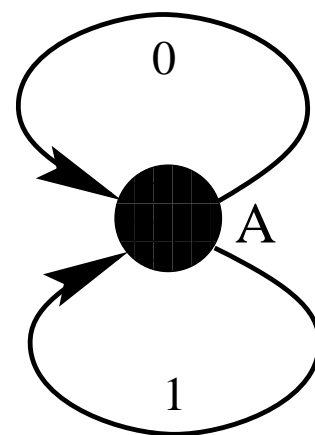


Fig. 1b

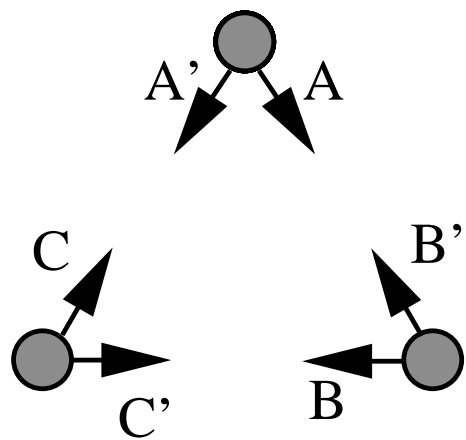


Fig. 2a

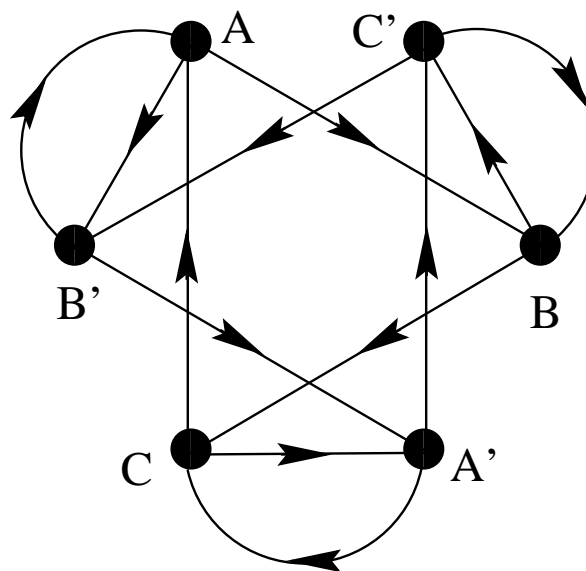
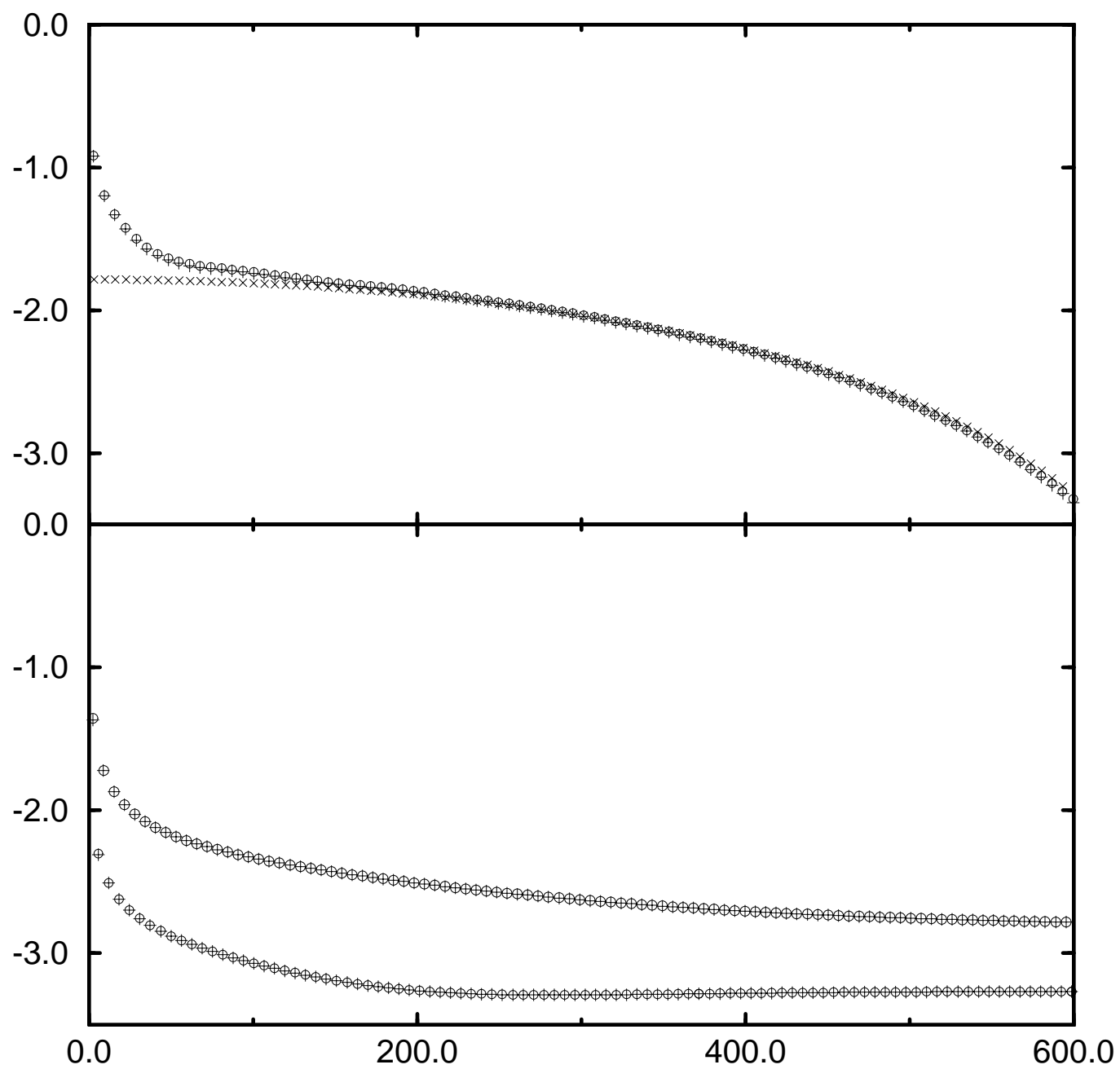


Fig. 2b



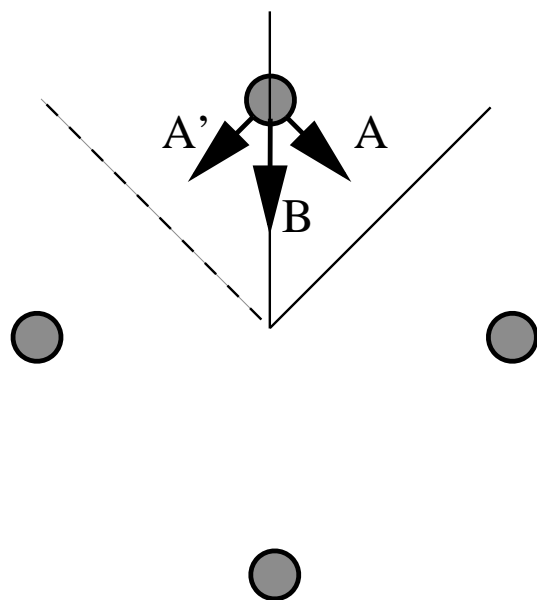


Fig. 4a

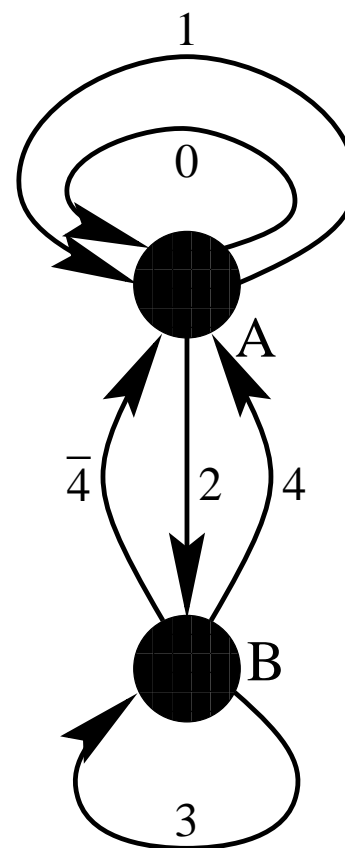


Fig. 4b

